Structural Plasticity of Functional Actin: Pictures of Actin Binding Protein and Polymer Interfaces

Heidi Rommelaere,* Davy Waterschoot,
Katrien Neirynck, Joël Vandekerckhove,
and Christophe Ampe
Flanders Interuniversity Institute
    for Biotechnology (VIB 09) and
Department of Biochemistry and Molecular Biology
Faculty of Medicine and Health Sciences
Ghent University
A. Baertsoenkaai 3
B-9000, Gent
Belgium

Summary

Actin is one of the most conserved and versatile proteins capable of forming homopolymers and interacting with numerous other proteins in the cell. We performed an alanine mutagenesis scan covering the entire β-actin molecule. Somewhat surprisingly, the majority of the mutants were capable of reaching a stable conformation. We tested the ability of these mutants to bind to various actin binding proteins, thereby mapping different interfaces with actin. Additionally, we tested their ability to copolymerize with α-actin in order to localize regions in actin that contact neighboring protomers in the filament. Hereby, we could discriminate between two existing models for filamentous actin and our data strongly support the right-handed double-stranded helix model. We present data corroborating this model in vivo. Mutants defective in copolymerization do not colocalize with the actin cytoskeleton and some impair its normal function, thereby disturbing cell shape.

Introduction

Actin is the major component of the microfilament system of eukaryotic organisms. As such, it plays a central role in cell motility processes. Actin is one of the most conserved proteins known today, and it is thought that its conserved nature reflects its strict structural requirement to interact with itself as well as with a variety of other proteins that modulate the transition between and the dynamics of the monomeric and polymeric state. For some actin binding proteins such as DNase I, profilin I, gelsolin, and the vitamin D binding protein, cocrystal structures exist (Kabsch et al., 1990; Schutt et al., 1993; McLaughlin et al., 1993; Robinson et al., 1999; Otterbein et al., 2002). For other actin modulator proteins, like thymosin β, the contact sites within actin have been proposed based on crosslinking and/or electron microscopy (EM) data (Safer et al., 1997; Ballweber et al., 2002). However, for the multitude of actin binding proteins (such as cyclase associated protein [CAP]) there are almost no data on actin interaction sites.

*Correspondence: heidi.rommelaere@ugent.be

Two actin filament models have been proposed. Holmes et al. (1990) constructed a filament using the atomic coordinates of the actin-DNase I complex fitted to X-ray fiber diffraction patterns obtained from oriented F(ilamentous)-actin gels. In this widely accepted model, actin protomers are associated in two strings, wound around each other in a right-handed helix. However, Schutt et al. argue that the ribbon like polymer, as observed in the actin profilin crystal (Schutt et al., 1993), could be the naturally occurring state of F-actin. The Holmes model was further refined by Lorenz et al. (1993), resulting in the identification of more extensive contacts between protomers, and was favored after an evaluation by Mendelson and Morris (1994). However, as pointed out by Mounier and Sparrow (1997), there is no in vivo evidence for either of the two models.

Mutational analysis of actins has been hampered because of its absolute requirement for the chaperonin CCT (cytosolic chaperonin containing TCP-1) to reach its native state (Gao et al., 1992; Rommelaere et al., 1993) and has been largely restricted to *Drosophila* and yeast actin (Hennessey et al., 1993). In particular, for the latter, the studies by Holtzman et al. (1994) and Wertman et al. (1992) show that actin mutations may specifically impair the interaction with an actin binding protein. However, these studies focused on clusters of charged residues only and analysis of genetic interactions. To probe the actin molecule and some of its functions more completely, we performed an alanine scan threading through the entire β-actin molecule substituting each time five consecutive amino acids. We established easy and reliable protocols for probing physical interactions of these mutants. As proof of principle, we tested the capacity of each of these mutants to bind to DNase I. We next compared data obtained from an interaction scan with adseverin, with data obtained from the crystal structures of actin in complex with gelsolin segments. Additionally, we assayed thymosin β4 and CAP to identify interaction regions in actin for these proteins. Finally, we investigated the ability of these actin mutants to copolymerize with α-actin. The data allowed us to evaluate the two existing models for the actin filament structure and are most consistent with the Holmes F-actin model. By expression of selected actin mutants in eukaryotic cells we also provide evidence that this model applies to the in vivo situation. In some cases noncopolymerizing mutants seem to act as filament cappers thereby affecting cell morphology.

Results and Discussion

For radioactively labeled wild-type actin produced in in vitro transcription translation reactions, interaction with various actin binding proteins can be monitored by a band-shift assay (Figure 1A) where an upward or downward shift of native monomeric actin can be observed, if after translation an actin binding protein is added. We note that relatively weak interactions (i.e., thymosin β4:

A

Wild type actin   Actin 60(A5)

B
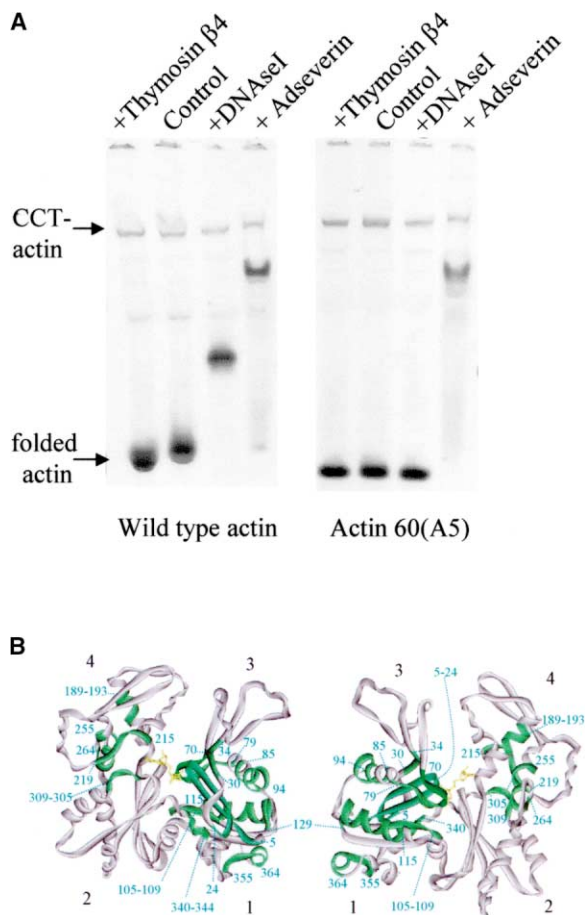
Figure 1. Actin Alanine Mutants, Folding Capacity, and Binding to Actin Binding Proteins

(A) Autoradiogram of a native gel analysis of ^{35}S-labeled β-actin or β-actin 60(A5) produced in an in vitro transcription translation reaction (control), band shifted with either thymosin β4, DNase I, or adseverin. Band shifts are also generated for interactions with relatively low K_D values (e.g., thymosin β4). It is, however, important that the actin binding protein is, like actin, attracted by the anode. (B) 3D structure of the actin fold (Kabsch et al., 1990) with in green those regions that, when mutated, cause folding defective mutants. In the right panel, the actin molecule is rotated by 180°. ATP is in yellow.

K_D 5 μM) can be monitored using this assay. We reasoned that, if the binding information for an actin binding protein in an actin mutant is removed or perturbed, such a band shift should not occur. We created 75 β-actin mutants in which we systematically replaced five consecutive amino acids by alanine (Table 1). We expressed these mutants in reticulocyte lysates, which endogenously contain the actin folding machines prefoldin and CCT (Gao et al., 1992; Rommelaere et al., 1993; Vainberg et al., 1998), and analyzed the ^{35}S-labeled products via native polyacrylamide gel electrophoresis. Fifty out of seventy-five mutants are able to fold and four remain associated with cyclase associated protein (CAP, see below and Table 1). In Figure 1B we show the regions that, when replaced by five alanines, cause folding defective actin molecules. As expected, these regions map mainly to the interior of the actin structure. These regions

may play a role in folding or may be important for generating a stable actin molecule. The chaperone interaction of these mutants will be described elsewhere (K.N. et al., unpublished data). We used the mutants that fold to investigate the interaction of actin with various actin binding proteins or with neighboring actin molecules in the filament.

The Alanine-Scan Mutants Allow Probing Interfaces with Actin Binding Proteins

To validate our assumption on band-shifting actin mutants, we first investigated binding to DNase I, since the contact sites in actin for this protein are known from the crystal structure. The major contact site consists of two loops in subdomain 2: the DNase binding loop 39–46 and the neighboring loop 61–64. The minor site is the loop containing residues 203–207 in subdomain 4 (Kabsch et al., 1990). Results of our band-shift assay show that actins mutated in the region 35–44 and 60–69 do not bind to DNase I, and actin mutated in region 45–49 binds less effective. Thus, this corresponds well with the major contacts observed in the actin-DNase complex (Figure 2A). However, actins mutated in region 203–207 are still able to bind to DNase, suggesting this region is less important in the contact, in agreement with the crystal structure.

We next investigated the actin binding protein adseverin. This gelsolin family member consists, like gelsolin, of six segments (S1–S6), has Ca^{2+}-dependent actin binding activity and is capable of binding two actin monomers (Robbens et al., 1998). In gelsolin, this occurs via S1 and via S4 as judged from crystal structures of monomeric actin either with S1 or with S4–S6 (McLaughlin et al., 1993; Robinson et al., 1999). Both segments interact with actin in a similar way by extensive contacts with subdomain 3 (residues 143, 144, 146–148, 167, 169, 296, 334) and additional contacts with subdomain 1 (residues 341, 345–346, 349–351, 354–355). If similar interactions hold for adseverin, our scan should reveal analogous regions. This is indeed what we observe. Using adseverin in the presence of Ca^{2+}, no band shifts are generated when regions 145–154, 165–169, and 295–299 in subdomain 3 are mutated (Figure 2B). The mutants 345(A5) and 350(A5) in subdomain 1 however did shift, but this may be due to the conserved character of the substitutions (the contacting residues are Ile, Leu, Ser, and Thr). Also, for 330(A5) a shift is observed, probably because Asp334 contributes little to the contact given its distance from the gelsolin molecule. Reduced binding is also seen for actins mutated in the regions 135–139, 300–304, 335–339, and 370–375. The latter four regions are spatially close to the interface residues and likely disturb local actin architecture (e.g., 300–304 is a central β strand in subdomain 3). Thus, these data on adseverin binding are in good agreement with the crystal contacts observed for gelsolin and suggest that adseverin contacts actin in a similar way as gelsolin, which is consistent with the conservation of the actin binding residues in of these proteins. Surprisingly, mutants 30(A5) and 50(A5) also produce no band shift. The mutated regions are located in subdomain 2, thus at the opposite site of the gelsolin S1 and S4 interface in actin. We suggest

that reduced binding of these mutants results from the conformational coupling that exists between the DNase I binding loop and the actin C terminus (Crosbie et al., 1994). Although possible allosteric communication between subdomains may complicate analysis, we conclude from the results with DNase I and adseverin that we can extract binding information for actin binding proteins with our band-shift assay, but only major contacts will be discovered and, not surprisingly, local conformational changes may affect binding.

An Extended Interface with Thymosin β4

Next we embarked on investigating proteins of which the interface with actin is controversial or unknown. So far, it has been impossible to obtain actin thymosin β crystals, but various models exist for the actin thymosin β interaction. The band-shift assay results show compromised binding for actins mutated in the regions 35–39, 60–74, 140–149, 194–198, 204–209, 300–304, 335–339, and 350–354 (Figure 2C). Mapped on the actin molecule, this reveals a remarkably extended area consistent with the elongated structure proposed for thymosin β4 in contact with actin (De La Cruz et al., 2000 [see Figure 8]; Safer et al., 1997). However, different from these studies, we do not find an interaction with the acidic actin N terminus. Thymosin β4 is even capable of stabilizing the conformation of two inherently unstable actin N-terminal deletion mutants (Rommelaere et al., 1999; Figure 2D). Based on two different crosslinking experiments, the N terminus of thymosin β is positioned near the subdomain 1-3 junction of actin (Safer et al., 1997; Reichert et al., 1996). Our results suggest that thymosin β4 binds between the helices 135–144 (subdomain 3) and 338–348 (subdomain 1) and passes across the actin ATP binding pocket toward the cleft between subdomains 2 and 4. Whereas this mode of binding deviates from the model proposed by Safer et al. (1997) with respect to the proposed interaction with the actin N terminus, it is in agreement with the results of Reichert et al. (1996) where thiol specific reagents were used to couple cysteine mutants of thymosin β to the C terminus of actin and to ATPγS. Also a recent model based on cryo-EM pictures of forced polymers of thymosin crosslinked actin positions thymosin β4 close to the ATP-cleft in actin (Ballweber et al., 2002 [see Figure 8B]). Although our results do not allow mapping exactly the thymosin β binding interface, they allow discrimination between different proposed binding models, obtained by other biochemical methods.

Cyclase-Associated Protein, CAP, Interacts with Actin in the Cleft between Subdomains 1 and 3

The band-shift assays above were performed in the presence of ATP. When ATP is omitted from the native gels, a new ^{35}S-labeled actin species, representing a complex between actin and endogenous CAP, appears in between the CCT-actin complex and hemoglobin (Figure 3A, lane 1; McCormack et al., 2001; mass spectrometry showed this is indeed an actin-CAP complex, data not shown). During the analysis of our actin mutants, we observed two phenotypes with respect to altered CAP binding. Either as noticed above for other actin binding proteins, mutants show diminished binding or, by contrast, some display a very pronounced increase in signal on native gels at the position of the actin-CAP complex (Figure 3A, lane 2). Folding competent actin molecules, with mutations in regions 140–154, 165–170, 280–299, 310–314, 335–339, 345–354, 365–374 do not bind to CAP suggesting that subdomains 1 and 3 form a large binding interface (Figure 3B; Table 1), which appears very similar to the vitamin D binding protein interaction site (Otterbein et al., 2002). However, mutation of residues 35–39 and 65–69 also influences CAP interaction. We note that the CAP-actin complex can bind to DNase I, but at higher DNase I concentration, CAP is chased from this complex (Figure 3A, lanes 3 and 4). This again indicates allosteric communication between subdomains 2 and 1 similar to what was observed above for adseverin. Mutations in subdomain 2 may freeze actin in a conformation incompetent for allowing interactions of actin binding proteins with the subdomain 1-3 binding cleft.

Actins Mutated in the ATP Binding Pocket Remain CAP Arrested

In the absence of ATP, CAP binding is increased for actin mutants 70(A5) 155(A5), 160(A5), 179(A5), 210(A5), and 300(A5) (Figure 3C; Table 1). Of these mutants, the latter five even bind to CAP when ATP is present in the gels, whereas under these conditions, no complex is observed for wild-type actin and other folding capable mutants. We observe normal binding to CAP when residues 15–19 and 135–139 are mutated whereas mutating residues surrounding these regions generates actins that do not bind to CAP. Interestingly, all these regions are located in or close to the ATP binding pocket of actin, and contain residues 16, 18, 137, 157–159, 213–214, and 302–303, which are all involved in divalent ion and ATP binding (Kabsch et al., 1990). This arrest on CAP may have serious effects on living cells since analogous mutants in yeast [154(A3), 210(A2), and 213(A3)] produce lethal or temperature sensitive phenotypes (Wertman et al., 1992) and mutating residues G156, G301 or G302 in the flight muscle actin of *Drosophila* result in abnormal myofibrils (An and Mogami, 1996). Additional residues involved in nucleotide interaction are 11, 14, 154, 305–306, and 336 (Kabsch et al., 1990). However actins with these residues mutated [10(A5), 150(A5), 305 (A5) and 335 (A5)] fail to form CAP complexes. Most probably, this is due to the fact that they are mutated close to or in the CAP interface or that they do not fold, since mutating single residues in one of the regions (D11A and S14A, McCormack et al., 2001) results in increased CAP binding.

Our results indicate CAP binding is sensitive to the nucleotide state of actin, hence CAP may be an actin binding protein involved in the stabilization of nucleotide free actin. Alternatively, a more active contribution of CAP in the actin folding pathway (Gao et al., 1992; Rommelaere et al., 1993; Vainberg et al., 1998) could be that it acts as an ATP-loading machine post-CCT. Thus, the actin alanine mutants provide important information on the actin interaction site with CAP and suggest clues on CAP function.

Table 1. Summary of the Folding Capacity of Actin Alanine Mutants and Binding to DNAse I, Adseverin, Thymosin β4, and CAP

Mutant	AA Changed	Folds	DNAse I	Adsev	Thym β4	CAP
actb(WT)		+	+	+	+	+
actb2(A3)	DDD	+	+	+	+	+
actb5(A5)	**IAALV**	−	−	+	−	−
actb10(A5)	VDNGS	−	−	+	−	−
actb15(A5)	GMCKA	−	−	weak	−	+
actb20(A5)	GFAGD	−	−	+	−	−
actb25(A5)	DAPRA	+	+	+	+	weak
actb30(A5)	VFPSI	−	−	weak	−	−
actb35(A5)	VGRPR	+	−	+/−	−	−
actb40(A5)	HQGVM	+	−	+	+	weak
actb45(A5)	VGMGQ	+	+/−	+	+	+
actb50(A5)	KDSYV	+	+	weak	+	+
actb55(A5)	GDEAQ	+	+	+	+	+
actb60(A5)	SKRGI	+	−	+	−	+
actb65(A5)	LTLKY	+	−	+/−	−	−
actb70(A5)	PIEHG	−	+	+	−	++
actb75(A5)	IVTNW	−	−	+	−	−
actb80(A5)	DDMEK	+	+	+	+	+
actb85(A5)	IWHHT	−	+	+	+	−
actb90(A5)	FYNEL	−	−	weak	−	−
actb95(A5)	RVAPE	+	+	+	+	+
actb100(A5)	EHPVL	(+)	+	+	weak	weak
actb105(A5)	LTEAP	−	−	weak	−	+
actb110(A5)	LNPKA	+	+	+	+	+
actb115(A5)	NREKM	−	−	+/−	−	−
actb120(A5)	TQIMF	−	−	−	−	−
actb125(A5)	ETFNT	−	−	?	−	−
actb130(A5)	PAMYV	+	+	+	+	weak
actb135(A5)	AIQAV	+	+	+/−	+	+
actb140(A5)	LSLYA	+	+	+	−†	−
actb145(A5)	SGRTT	+	+	−	−	−
actb150(A5)	GIVMD	(+)	+	−	+	−
actb155(A5)	SGDGV	CAP	+	+	+	+++
actb160(A5)	THTVP	+	+	+	+	++
actb165(A5)	IYEGY	+	+	−	+	−
actb170(A5)	ALPHA	+	+	+	+	weak
actb175(A5)	ILRLD	+	+	+	+	+
actb179(A5)	DLAGR	(+)	−	weak	−	++
actb184(A5)	DLTDY	+	+	+	+	+
actb189(A5)	LMKIL	−	−	−	−	−
actb194(A5)	TERGY	+	+	+	−	+
actb199(A5)	SFTTT	+	+	+	+	+
actb204(A6)	AEREIV	+	+	++	−	+
actb210(A5)	RDIKE	CAP	+	+	+	+++
actb215(A5)	KLCYV	−	−	−	−	−
actb220(A5)	ALDFE	+	+	+	+	+
actb225(A5)	QEMAT	+	+	+	+	+
actb230(A5)	AASSS	+	+	+	+	+
actb235(A5)	SLEKS	+	+	+	+	+
actb240(A5)	YELPD	+	+	+	+	+
actb245(A5)	GQVIT	+	+	+	+	+
actb250(A5)	IGNER	+	+	+	+	+
actb255(A5)	FRCPE	−	−	−	−	−
actb260(A5)	ALFQP	−	−	−	−	−
actb265(A5)	SFLGM	+	+	+	+	+
actb270(A5)	ESCGI	+	+	+	+	+
actb275(A5)	HETTF	+	+	+	+	+
actb280(A5)	NSIMK	+	+	+	+	weak
actb285(A5)	CDVDI	+	+	+	+	−
actb290(A5)	RKDLY	+	+	+	+	−
actb295(A5)	ANTVL	+	+	−	+	−
actb300(A5)	SGGTT	CAP	+	weak	−	++
actb305(A5)	MYPGI	−	−	−	−	−
actb310(A5)	ADRMQ	(+)	+	+	+	−
actb315(A5)	KEITA	+	+	+	+	+
actb320(A5)	LAPST	+	+	+	+	+
actb325(A5)	MKIKI	+	+	+	+	+

Table 1. Continued

Mutant	AA Changed	Folds	DNAse I	Adsev	Thym β4	CAP
actb330(A5)	IAPPE	+	+	+	+	+
actb335(A5)	RKYSV	+	+	+/−	−	−
actb340(A5)	WIGGS	−	−	−	−	−
actb345(A5)	ILASL	+	+	+	+	−
actb350(A5)	STFQQ	+	+	+	−	weak
actb355(A5)	MKISK	−	−	−	−	−
actb360(A5)	QEYDE	−	−	−	−	−
actb365(A5)	SGPSI	+	+	+	+	−
actb370(A6)	VHRKCF	+	+	weak	+	−

+ indicates that the mutant folds or interacts with the listed binding protein; (+) indicates only a small part of the population is folded; +/−
is reduced binding. CAP indicates the mutant is arrested on cyclase associated protein even in the presence of atp.
− indicates lack of folding or binding
++ and +++ indicate increased CAP binding.

In Vitro Actin Polymerization Supports the Holmes F-Actin Model

Since we could locate regions in actin important for interaction with actin binding proteins, we hypothesized that we could also identify actin-actin contacts between neighboring protomers in the actin filament. Two major F-actin models have been proposed which we will refer to as the Holmes model and the ribbon model. The first model is based on low-resolution diffraction data of oriented F-actin filaments (Holmes et al., 1990) and is widely accepted because it is consistent with numerous biochemical experiments (e.g., Steinmetz et al., 1998).
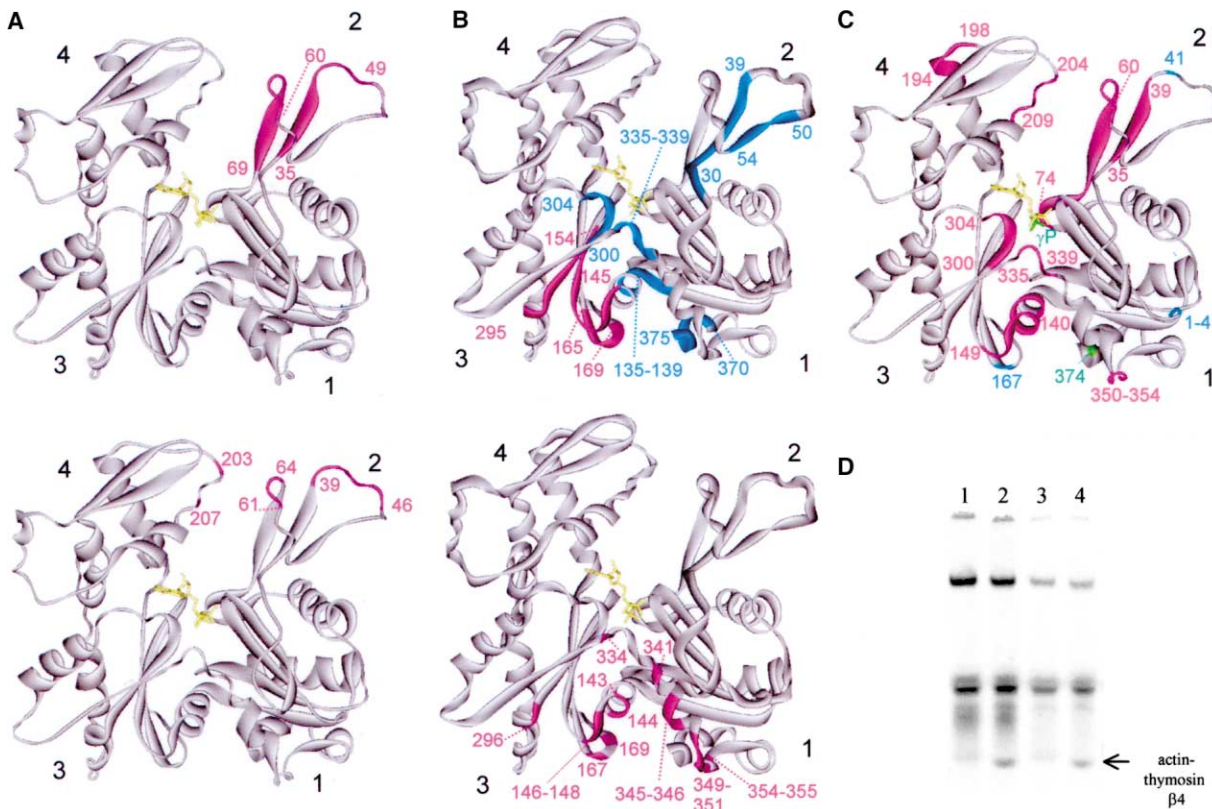

Figure 2. Residues of Actin Important for Binding to DNase I, Adseverin, and Thymosin β

(A–C) 3D structures of actin showing a comparison of our interaction scan results (upper molecules) with data from X-ray structures (lower molecules, Kabsch et al., 1990; McLaughlin et al., 1993; Robinson et al., 1999) or models. The regions important for interaction with the respective actin binding proteins are indicated in pink.
(A) The DNase I interface, (B) the gelsolin/adseverin S1 and S4 interfaces (pink: mutants with loss of binding, blue: mutants with reduced binding), (C) model of thymosin β4 interaction, pink: our results, blue: crosslinked residues (Safer et al., 1997), green: thiol crosslinked residues (Reichert et al., 1996), γP represents the γ-phosphate moiety of ATP-γS.
(D) Thymosin β4 is able to bind to actin lacking its N terminus. Autoradiogram of a native gel analysis of ^{35}S-labeled actin(Δ1–5) (lanes 1 and 2) and actin(Δ1–6) (lanes 3 and 4) produced in an in vitro transcription translation reaction, band shifted with thymosin β4 (lanes 2 and 4). Note these mutants are unstable and only form a discrete band when complexed to thymosin β4 (compare with wild-type actin in Figure 1A).

A

B

C
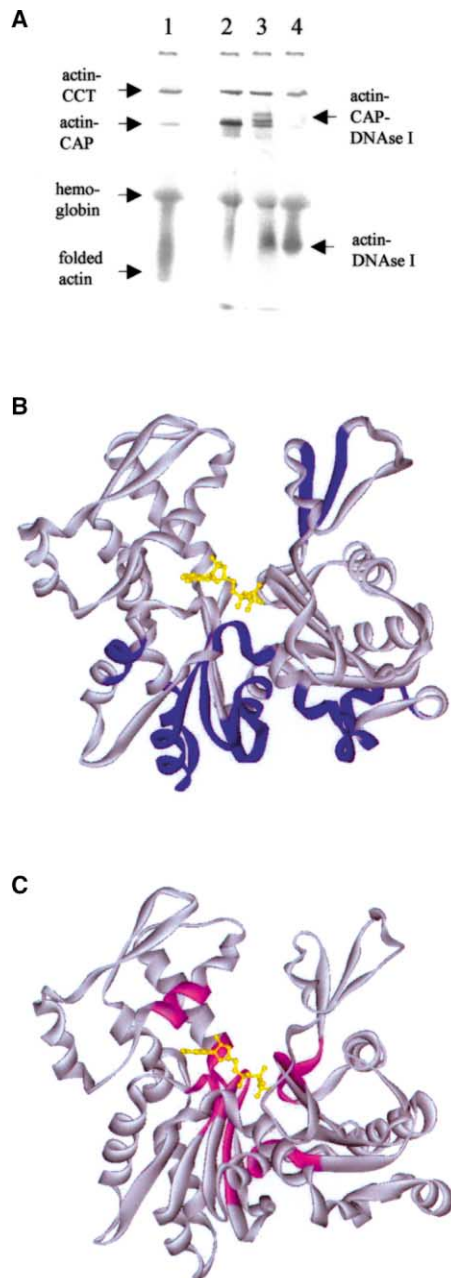
Figure 3. CAP Binds in the Subdomain 1–3 Cleft of Actin and Mutating Residues Involved in ATP Binding Stabilizes the CAP Actin Interaction

(A) Autoradiogram of a native gel analysis without ATP of ^{35}S-labeled actin (lane 1) and actin 155(A5) (lanes 2-4) produced in an in vitro transcription translation reaction. DNase I can form a ternary complex with the actin-CAP complex (lane 3, 0.25 nM DNaseI added) or can compete with CAP for actin binding when added at higher concentrations (lane 4, 8.25 nM DNaseI added). CAP is dimeric (unpublished observation), hence can bind two actin molecules resulting in two shifts with DNase I. Note that in gels without ATP, folded actin does not run as a discrete band.

(B) Actins with mutation in one of the purple colored regions in the 3D-structure show decreased binding to CAP suggesting the latter binds in the cleft between subdomains 1 and 3.

(C) Actins with mutation in one of the regions indicated in pink show increased binding to CAP. These regions are involved in ATP binding.

However, the ribbon model is intriguing because it is observed in the high-resolution profilin-actin crystal structure (Schutt et al., 1993). In the Holmes model, actin protomers are associated in two strings wound around each other in a right-handed helix, with interactions along and across the strands. The interactions between molecules along one strand involve contacts between subdomain 4 and subdomain 2 of one protomer with subdomain 3 of the next. Contacts across the two strands are made between subdomain 1 of one protomer and subdomain 4 of the other and by the so-called hydrophobic plug which inserts into a hydrophobic pocket (Holmes et al., 1990; for a detailed list of residues involved see legend of Figure 4A). In the ribbon model (Schutt et al., 1993), subdomain 4 and the upper part of subdomain 2 of one protomer contact subdomain 1 and the lower part of subdomain 2 of the next (Figure 4B).

Regions common to the two models are 40–45, 60–64, 202–205, and 243–245; thus these regions are not informative for discrimination. The main differences between the models are, however, that in the ribbon subdomain 1 is involved in the contact whereas in the Holmes model this is subdomain 3 with additionally the hydrophobic plug contact (Figures 4A and 4B; Table 2). More concrete, residues involved in the Holmes but not in the ribbon model are 39, 110–112, 166–169, 171, 173, 195–197, 266–270, 285–289, 322–325, and 375 and vice versa residues involved in the ribbon but not in the Holmes model are 2–5, 48–50, 87–97, 99–100, 130–131, and 353–360.

To distinguish between the two models, we tested if the actin alanine mutants were able to copolymerize with purified α-skeletal muscle actin. Two mutants [100(A5) and 310(A5)] were prone to aggregation during the assay suggesting decreased stability. They are not taken up in the argumentation below. All nondiscriminative mutants (i.e., in the region 60–69, 199–203, 204–209, and 240–244) are defective or affected in copolymerization. More importantly, mutations in the regions 35–39, 165–169, 194–199, 285–289, and 325–329 solely predicted in the Holmes model, lead to loss in copolymerization [35(A5), 165(A5) and 285(A5)], or result in reduced copolymerization capacity [194(A5) and 325(A5); Table 2; Figure 4C]. By contrast, mutants in the region 45–49, 50–54, 95–99, 130–134, and 350–354, characteristic for the contacts in the ribbon model, display wild-type or nearly wild-type copolymerization capacity [mutants 85(A5), 90(A5) and 355(A5) do not fold]. Thus, these results strongly favor the Holmes model. Moreover, actin mutants 35(A5) en 285(A5) appear to act as filament capping molecules when transfected in eukaryotic cells (see below), suggesting actin 35(A5) is crucial at the pointed and actin 285(A5) at the barbed end, which can only be explained in the Holmes model. We also find impaired copolymerization capacity for mutants in regions structurally close to a major contact in the Holmes model. Possibly mutations in these neighboring regions influence correct positioning of the F-actin contacts. For instance, mutants 275(A5), 280(A5), 290(A5), and 295(A5) are close to the 285–289 loop and mutants 145(A5) and 150(A5) comprize a core β strand in subdomain 3 that is close to the predicted Holmes contact regions 166–169 and 171–173. Similarly, mutating the region 220-224
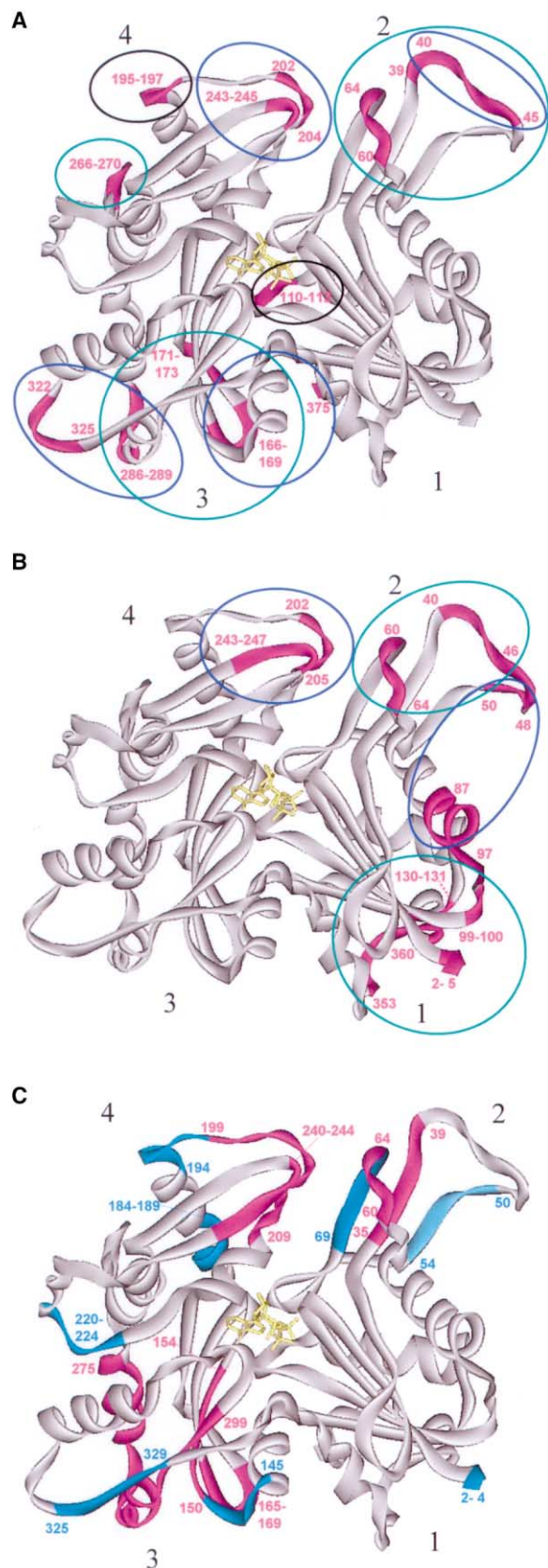
may influence correct positioning of the hydrophobic plug. Also, the reduced copolymerization capacity of 184(A5), having mutations in the core of a helix, can be explained this way. However, at present it is not clear whether this mutation affects the correct positioning of the F-actin contact 195–197 at the end of this helix or loop 266–272 that is structurally nearby. Only the behavior of the mutant 2(A3) does not fit the Holmes model and this region is actually a predicted ribbon model contact. This mutant has reduced copolymerization activity, which we currently cannot explain. However we stress that the other discriminating mutants, covering major contacts predicted in the ribbon model, are fully capable of polymer formation.

The severity of the copolymerization phenotypes of the actin mutants correlate well with the critical contacts proposed in the Holmes model. Changing residues in regions participating simultaneously in contacts along and across the helix (residues in the intersections of the blue and green circles in Figure 4A) result consistently in mutants that are dramatically compromised in copolymerization. Actin mutants with substitutions of residues involved in only one type of contact are either severely, or little or not affected in their copolymerization capacity. This observation may indicate that the latter regions are less important for polymer formation. We often find that mutations in regions, adjacent to proposed contact sites in the Holmes model, also cause defective copolymerization. This may be suggestive of more extensive contacts as proposed in the refined version of the Holmes model (Lorenz et al., 1993). In addition, we note that, in fitting the actin X-ray structure to the 8.4 Å fiber diffraction data, domain movements were allowed (Holmes et al., 1990) and in the subsequent refined model, loops were rebuilt (Lorenz et al., 1993).

In summary, our results from the in vitro copolymeriza-

Figure 4. Actin Residues Important for Polymerization

(A and B) 3D representation of actin with highlighted in pink the residues important in the F-actin contacts according to the two F-actin models.

(A) In the right-handed helix model of Holmes et al. (1990), interactions between molecules along one strand involve contacts between subdomain 4 and subdomain 2 of one protomer with subdomain 3 of the next, i.e., residues 243–245 contact 322–325, 202–204 contact 286–289, and 41–45 contact 166–169 and 375 (blue circles). Arg 39 is possibly involved in a salt bridge with Asp 286 and Glu 270, each in a different actin molecule. Contacts across the two strands occur between subdomain 1 residues 110–112 of one protomer and 195–197 in subdomain 4 of the other (black circles). In addition a loop, the so called hydrophobic plug (266–269) is suggested to insert across the helix into a hydrophobic pocket formed by residues 166, 169, 171, 173, 285, 289 and residues 40–45, 63 and 64 of two adjacent protomers in one strand (green circles).

(B) In the zigzag ribbon model (Schutt et al., 1993), residues 40–42, 44–46, and 60–64 of subdomain 2 of one protomer contact residues 2, 4, 5, 99, 100, 130, 131, 353, 358, and 360 of subdomain 1 of the next (green circles). In addition residues 202, 204, 205, and 243–247 of subdomain 4 from the lower protomer contact residues 48, 50, 87, 91, 92, 95, and 97 of subdomain 2 of the upper (blue circles).

(C) 3D representation of actin showing regions important for copolymerization as deduced from our in vitro copolymerization assay. Alanine substitutions of the colored regions result in actin mutants that do not copolymerize (pink) or that have reduced copolymerization activity (blue).

tion assays can best be explained in terms of the Holmes model for the actin filament (or the Lorenz version of it). The experiments also illustrate the power of our approach in complementing and validating modeling data, performed at lower resolution range.

In Vivo Evidence for the Holmes F-Actin Model

The copolymerization assay above inherently uses a large excess of carrier wild-type actin and does not allow investigation of more subtle effects on actin filaments. Moreover, as yet, there is no evidence that in vivo polymer contacts are the same as those predicted from the models (Mounier and Sparrow, 1997). Therefore, we investigated the behavior of selected Myc-tagged actin mutants in NIH3T3, NG108, or Hek293T cells. Only the results for NIH3T3 cells are shown, but all cell types gave similar results. The actin cytoskeleton was stained with phalloïdin-alexa red, and the actin mutants were detected with an anti-Myc FITC antibody. As a control we introduced Myc-tagged wild-type actin, which nicely incorporates in the actin filaments (Figure 5A), also the copolymerizing 345(A5) mutant colocalizes with actin filaments (Figure 5B). Mutants 60(A5), 35(A5), 285(A5), 145(A5), and 295(A5), defective in copolymerization in vitro and fitting the Holmes model, do not colocalize with actin filaments (Figures 5C–5G). By contrast, mutants 95(A5) and 350(A5), that do copolymerize (see above) and cover predicted contacts in the ribbon model, are incorporated in filaments (Figures 5H and 5I). Transfected cells expressing the polymerization defective mutants 145(A5) and 295(A5), which have mutations in regions peripheral to the contacts proposed in the Holmes model, have a normal cytoskeleton and shape (Figures 5F and 5G). For mutants in the interaction regions, we observed different phenotypes with regard to actin cytoskeleton and cell shape. Mutants 60(A5) and 35(A5) induce in many cases formation of densely stained actin fibers in the center of the cells with some residual F-actin staining in a punctuate pattern in case of mutant 35(A5) (Figures 5C, 5D, and 6). The dense short actin fibers formed in 60(A5) transfected cells are not in the nucleus, as can be seen in Figure 6C. The nucleus itself appears also reduced and deformed. In most cases, the transfected cells are much smaller and rounded, likely due to the collapse of the actin cytoskeleton, which may explain why most of these transfectants were lost after 48 hr. Cells transfected with 285(A5) seem to have an intermediate phenotype. They are again much smaller and we observed reduced staining of F-actin fibers, although the effect on the cytoskeleton is less severe compared to cells transfected with mutants 60(A5) and 35(A5) (Figure 5E). At present, we can only speculate on the cause of this severe phenotype. On the one hand an interaction with an organizing actin binding protein may be compromised, but perhaps more likely, the disturbance of the cytoskeleton is caused by a continuously filament capping action of these mutants. Indeed, regions 35–49 and 60–64, and 285–289 are on opposite sides of the actin protomer and, if located in an F-actin contact, mutants in these regions may behave as actin filament capping proteins and will affect actin dynamics with pointed end mutants having a stronger effect. As

Table 2. Copolymerization Capability of Actin Alanine Mutants that Fold

| Mutant	Copol	Holmes	Ribbon
actb(WT)	+		
actb2(A3)	+/−		X
actb25(A5)	+		
actb35(A5)	−	/	
actb40(A5)	+	X	X
actb45(A5)	+	/	X
actb50(A5)	++/−		/
actb55(A5)	+		
actb60(A5)	−	X	X
actb65(A5)	+/− −		
actb80(A5)	+		
actb95(A5)	+		X
actb110(A5)	+	X	
actb130(A5)	+		X
actb135(A5)	++		
actb140(A5)	+		
actb145(A5)	+/−		
actb150(A5)	−		
actb160(A5)	+		
actb165(A5)	−	X	
actb170(A5)	+	X	
actb175(A5)	+		
actb184(A5)	+/−		
actb189(A5)			
actb194(A5)	+/−	X	
actb199(A5)	−	X	X
actb204(A6)	−	/	X
actb220(A5)	+/−		
actb225(A5)	+		
actb230(A5)	+		
actb235(A5)	+		
actb240(A5)	−	X	X
actb245(A5)	+	/	X
actb250(A5)	+		
actb265(A5)	+	X	
actb270(A5)	+	/	
actb275(A5)	−		
actb280(A5)	−		
actb285(A5)	−	X	
actb290(A5)	−		
actb295(A5)	−		
actb315(A5)	+		
actb320(A5)	+	X	
actb325(A5)	+/−	/	
actb330(A5)	+		
actb335(A5)	+		
actb345(A5)	+		
actb350(A5)	+		X
actb365(A5)	+		
actb370(A6)	+	/	

X indicates that several amino acids in this region are involved in the Holmes, respectively ribbon model, / indicates that only one amino acid in this region is involved.

− indicates folded mutants that do not copolymerize.

++/−, +/−, and +/−− indicate different levels of reduced copolymerization activity.

the Holmes model predicts that regions 35–39 and 60–64 are at the minus end and 285–289 is at the plus end, our in vivo data again support this model. Unfortunately, our in vitro polymerization assay described above was not sensitive enough to detect capping activity for actin 60(A5) and 285(A5), however for 35(A5) we noticed capping activity in vitro (data not shown). The results obtained with the latter mutants may also explain the tem-
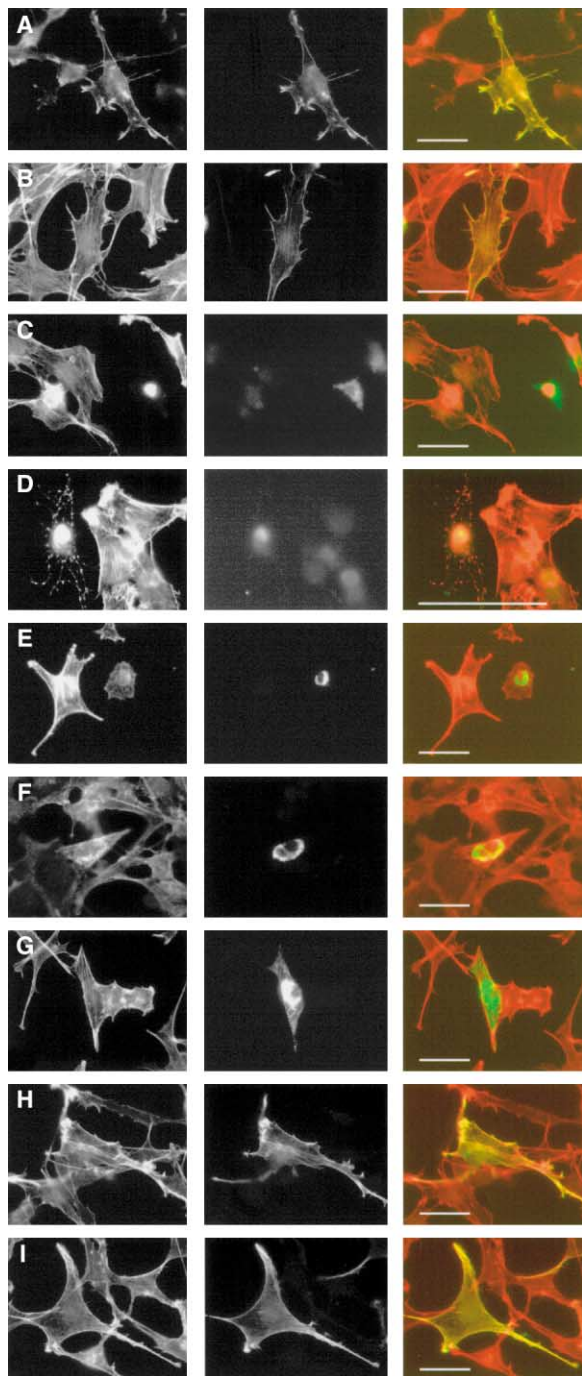
Figure 5. In Vivo Evidence for the Holmes Model

Expression of N-terminally Myc-tagged actin alanine mutants in NIH 3T3 cells. Western blotting of lysates of transfected cells and probing with mouse anti-Myc antibodies revealed the presence of actins with the correct molecular weight (data not shown). (A) Wild-type actin, (B) actin 345(A5), (C) actin 60(A5), (D) actin 35(A5), (E) actin 285(A5), (F) actin 145(A5), (G) actin 295(A5), (H) actin 95(A5), and (I) actin 350(A5). Left panels are phalloïdin staining of the actin cytoskeleton, middle panels, anti-Myc-FITC staining of the expressed mutants, right panels overlay (phalloïdin = red, myc = green). (A) and (B) are controls were one can observe incorporation of in vitro copolymerizable Myc-tagged actins. For the mutants shown in (C)–(G), Holmes contacts are disturbed and no incorporation of Myc-actin mutants is observed. In (C) and (E), transfected cells are smaller

perature sensitivity, respectively lethality of the yeast actin mutants 37(A3), 61(A2), and 286(A3) (Wertman et al., 1992) and the disruption of indirect flight muscle fibers by the G63D mutation in *Drosophila* (An and Mogami, 1996). Mutating the 93–95 and the 99–100 regions in yeast also results in a strong phenotype, although we do not observe defects in copolymerization for the 95(A5) mutant. In this case the effects observed in yeast (and also in *Drosophila*) are probably caused by the fact that myosin and/or fimbrin binding contacts are disturbed (Wertman et al., 1992; Holtzman et al., 1994; Razzaq et al., 1999). The severity of disrupting these contacts is likely dependent on the cell type or on the growth conditions.

In summary, both our in vitro and in vivo experiments support the Holmes model for actin filaments.

Conclusion
In view of the conservation of actin, it is remarkable that so many regions of this molecule can be changed without having deleterious effects in vitro. Indeed only a minority of the mutants does not fold or is extremely unstable suggesting larger than expected structural plasticity of the actin molecule. Therefore, the reason for this extreme conservation may indeed be the number of different interactions actin participates in. Hence our mutants are important tools for extracting binding information on interaction with its partners, as we did for adseverin, thymosin β, CAP and actin itself. Additionally, the mutants can be helpful in gathering information on the function of actin binding partners, since we found, unexpectedly, that CAP may stabilize nucleotide free actin. With regard to actin filament contacts, our results show that actins mutated in contact regions predicted in the Holmes model fail to copolymerize in vitro and do not colocalize with endogenous actin in cells and, in some cases, even disturb the actin cytoskeleton. On the other hand mutants in predicted ribbon contacts appear to have no effects on cell morphology and colocalize with the endogenous actin. In addition, by creating these mutants and developing an analysis system we established a platform to address more easily questions with respect to actin mutants in muscle diseases like dilated cardiomyopathy (Olson et al., 1998), and nemaline myopathy (Nowak et al., 1999; Ilkovski et al., 2001) or actin mutants associated with neutrophil dysfunction (Nunoi et al., 1999) or tumorigenesis (Lin et al., 1985). Obviously, it would be interesting to investigate the supra-molecular structure of filaments harboring mutant actin molecules, by electron microscopy or their effect on actin dynamics. However, given the relatively low levels of protein produced in the transcription/translation assay this is a future objective, as these experiments require generating sufficient amounts of mutant actin.

and in (C) and (D), the endogenous actin filamentous network is even disturbed and cells loose their shape (see also more detailed in Figure 6). The mutants shown in (H) and (I) incorporate in the filaments which disagrees with the ribbon model. Scale bar = 40 μm.
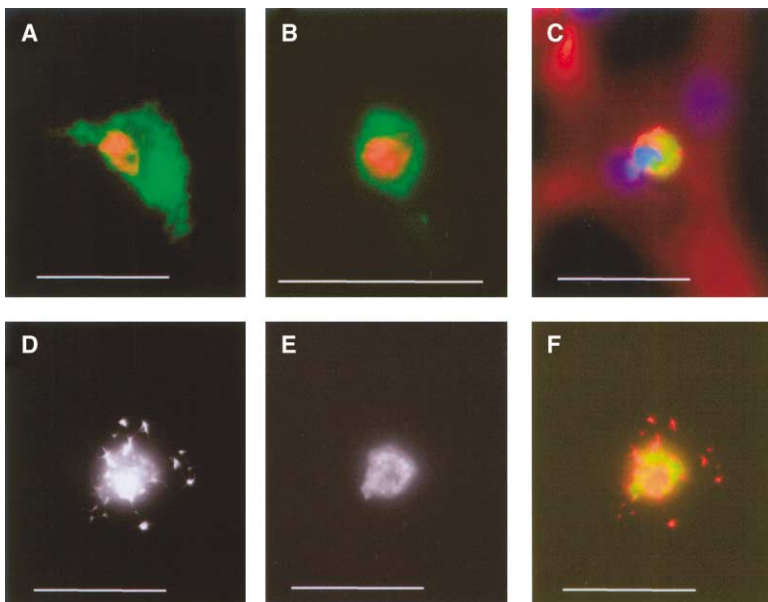
Figure 6. Introduction of Noncopolymerizing Actin Mutants in Cells Has Drastic Effects on the Cytoskeleton and Cell Shape

(A–C) Details of three different transfected NIH3T3 cells with Myc-tagged actin mutants 60(A5), (A) is a detail of Figure 5C. Green is anti-Myc, red is phalloïdin, and blue is DAPI staining (only in [C]). Actin filaments (red) appear as extranuclear short thick fibers, the nucleus seems to be smaller and deformed. (D–F) Detail of a cell transfected with Myc-tagged actin 35(A5), (D) is phalloïdin staining, (E) is anti-Myc staining, and (F) is the overlay. In all images the scale bar is 20 μm.

Experimental Procedures

Construction of the β-Actin Alanine Mutants

Alanine-scan mutants were made with the Quik Change site directed mutagenesis kit (Stratagene) using human β-actin in pcDNA3.1 (Invitrogen) as a template. The primers were designed in such a way that five consecutive codons are changed to codons for alanine and that a PstI restriction site is introduced. This enabled rapid checking for introduction of mutations. N-terminal Myc-tagged wild-type and actin mutants were made by PCR using the actin-alanine mutants in the pcDNA3.1 vector as template, a 5′ primer containing the myc-sequence preceded by a HindIII site and a 3′ primer containing a XbaI site. These fragments were ligated in HindIII-XbaI digested pcDNA3.1. Constructs were sequenced at the 5′ and/or 3′ end of their coding sequence and the alanine-scan mutants at the site of the introduced mutations.

Expression of Actin Alanine Mutants and Band-Shift Assays with Actin Binding Proteins

We expressed the actin alanine mutants as ^{35}S-labeled proteins in in vitro transcription translation reactions in reticulocyte lysate (Promega) according to the manufacturer's instructions, using 0.02 μCi ^{35}S-methionine (ICN) and 200 ng DNA per 25 μl reaction. After incubation at 30°C for 1.5 hr, we analyzed the reaction products on denaturing tricine gels (Schagger and von Jagow, 1987) and on nondenaturing polyacrylamide gels according to Safer (1989) with ATP, followed by auto radiography. To monitor CAP binding, ATP was omitted from the gels. The amount of ^{35}S-actin bound to CAP was quantified by phosphor imaging (Typhoon 9200 variable mode imager, Amersham Biosciences) and the ImageQuant software package. For the band-shift assays, 1 μl of the respective actin binding proteins was added to 3 μl of the in vitro transcription translation reaction. After 1 min incubation the mixture was analyzed on native gels with 200 μM ATP, or in the case of adseverin with 200 μM ATP and 200 μM Ca^{2+}. The final concentration of the respective actin binding proteins was 2 nM for DNase I, 12.5 nM for thymosin β4, and 1 nM for adseverin. These concentrations are the minimal amounts of the actin binding proteins needed to cause a band shift of wild-type actin, as was determined by a concentration series. Binding capacity was inspected by eye. Reduced or less effective binding means that only a part of the population of the mutant actin molecules shifted, and part remain unshifted.

DNase I was purchased from Worthington. Thymosin β4 was chemically synthesized on a model 431A peptide synthesizer using solid phase Fmoc chemistry. Adseverin was recombinantly expressed and purified according to Robbens et al. (1998).

Polymerization Assays

Twenty-five microliters of an in vitro transcription translation reaction of wild-type or mutant β-actin was centrifuged at 100,000 rpm in a Beckman airfuge to remove aggregates. To the supernatant, we added 25 μl of 12 μM α-actin (purified from rabbit skeletal muscle according to Pardee and Spudich [1982]) in G buffer (2 mM Tris-HCl [pH 8], 0.2 mM CaCl$_2$, 0.5 mM DTT, 0.2 mM ATP), i.e., approximately a 500-fold excess of α-actin over mutant β-actin. We adjusted the buffer conditions to 100 mM KCl and 1 mM MgCl$_2$ (F-buffer) and allowed the actin to polymerize for 2 hr at room temperature. F-actin was pelleted by centrifugation at 100,000 rpm for 20 min. The supernatant was removed (supernatant 1), the pellet washed and resuspended in 80 μl G buffer. Actin was allowed to depolymerize overnight at 4°C. A second round of polymerization was induced for 2 hr. F-actin was again centrifuged at 100,000 rpm for 20 min, which resulted in the final pellet from which the supernatant 2 was removed. Aggregates, supernatant 1 and 2 and the final pellet were analyzed on a 12.5% SDS-gel followed by auto radiography. The amount of ^{35}S-labeled actin in each fraction was quantified using phosphor imaging. All mutants were analyzed at least three times.

In Vivo Localization

We transfected pcDNA3.1 vectors encoding N-terminally Myc-tagged β-actin (wild-type or mutant) in NIH 3T3 fibroblast cells using electroporation. Twenty-four hours after transfection, cells were washed with PBS and fixed with 3% paraformaldehyde, permeabilized with 0.1% Triton X100 in PBS and incubated for 1 hr at room temperature with an anti-Myc-FITC antibody (Invitrogen) and phalloïdin-alexa-red (Molecular Probes). In some cases, additional DAPI staining was applied (0.4 μg/ml). Stained cells were examined using a Zeiss Axioplan II epifluorescence microscope equipped with a X40 and a X63 objective. Images were taken using a cooled CCD Axiocam Camera and KS100 software (Zeiss). Native gel analysis of in vitro transcription translation reactions of these N-terminally tagged wild-type and mutant actins show they behave like their nontagged versions.

References

An, H.S., and Mogami, K. (1996). Isolation of 88F actin mutants of Drosophila melanogaster and possible alterations in the mutant actin structures. J. Mol. Biol. *260*, 492–505.

Ballweber, E., Hannappel, E., Huff, T., Stephan, H., Haener, M., Taschner, N., Stoffler, D., Aebi, U., and Mannherz, H.G. (2002). Polymerisation of chemically cross-linked actin:thymosin beta(4) complex to filamentous actin: alteration in helical parameters and visualisation of thymosin beta(4) binding on F-actin. J. Mol. Biol. *315*, 613–625.

Crosbie, R.H., Miller, C., Cheung, P., Goodnight, T., Muhlrad, A., and Reisler, E. (1994). Structural connectivity in actin: effect of C-terminal modifications on the properties of actin. Biophys. J. *67*, 1957–1964.

De La Cruz, E.M., Ostap, E.M., Brundage, R.A., Reddy, K.S., Sweeney, H.L., and Safer, D. (2000). Thymosin-beta(4) changes the conformation and dynamics of actin monomers. Biophys. J. *78*, 2516–2527.

Gao, Y., Thomas, J.O., Chow, R.L., Lee, G.H., and Cowan, N.J. (1992). A cytoplasmic chaperonin that catalyzes beta-actin folding. Cell *69*, 1043–1050.

Hennessey, E.S., Drummond, D.R., and Sparrow, J.C. (1993). Molecular genetics of actin function. Biochem. J. *291*, 657–671.

Holmes, K.C., Popp, D., Gebhard, W., and Kabsch, W. (1990). Atomic model of the actin filament. Nature *347*, 44–49.

Holtzman, D.A., Wertman, K.F., and Drubin, D.G. (1994). Mapping actin surfaces required for functional interactions in vivo. J. Cell Biol. *126*, 423–432.

Ilkovski, B., Cooper, S.T., Nowak, K., Ryan, M.M., Yang, N., Schnell, C., Durling, H.J., Roddick, L.G., Wilkinson, I., Kornberg, A.J., et al. (2001). Nemaline myopathy caused by mutations in the muscle alpha-skeletal- actin gene. Am. J. Hum. Genet. *68*, 1333–1343.

Kabsch, W., Mannherz, H.G., Suck, D., Pai, E.F., and Holmes, K.C. (1990). Atomic structure of the actin:DNase I complex. Nature *347*, 37–44.

Lin, C.S., Ng, S.Y., Gunning, P., Kedes, L., and Leavitt, J. (1985). Identification and order of sequential mutations in beta-actin genes isolated from increasingly tumorigenic human fibroblast strains. Proc. Natl. Acad. Sci. USA *82*, 6995–6999.

Lorenz, M., Popp, D., and Holmes, K.C. (1993). Refinement of the F-actin model against X-ray fiber diffraction data by the use of a directed mutation algorithm. J. Mol. Biol. *234*, 826–836.

McCormack, E.A., Rohman, M.J., and Willison, K.R. (2001). Mutational screen identifies critical amino acid residues of beta-actin mediating interaction between its folding intermediates and eukaryotic cytosolic chaperonin CCT. J. Struct. Biol. *135*, 185–197.

McLaughlin, P.J., Gooch, J.T., Mannherz, H.G., and Weeds, A.G. (1993). Structure of gelsolin segment 1-actin complex and the mechanism of filament severing. Nature *364*, 685–692.

Mendelson, R.A., and Morris, E. (1994). The structure of F-actin. Results of global searches using data from electron microscopy and X-ray crystallography. J. Mol. Biol. *240*, 138–154.

Mounier, N., and Sparrow, J.C. (1997). Structural comparisons of muscle and nonmuscle actins give insights into the evolution of their functional differences. J. Mol. Evol. *44*, 89–97.

Nowak, K.J., Wattanasirichaigoon, D., Goebel, H.H., Wilce, M., Pelin, K., Donner, K., Jacob, R.L., Hubner, C., Oexle, K., Anderson, J.R., et al. (1999). Mutations in the skeletal muscle alpha-actin gene in patients with actin myopathy and nemaline myopathy. Nat. Genet. *23*, 208–212.

Nunoi, H., Yamazaki, T., Tsuchiya, H., Kato, S., Malech, H.L., Matsuda, I., and Kanegasaki, S. (1999). A heterozygous mutation of beta-actin associated with neutrophil dysfunction and recurrent infection. Proc. Natl. Acad. Sci. USA *96*, 8693–8698.

Olson, T.M., Michels, V.V., Thibodeau, S.N., Tai, Y.S., and Keating, M.T. (1998). Actin mutations in dilated cardiomyopathy, a heritable form of heart failure. Science *280*, 750–752.

Otterbein, L.R., Cosio, C., Graceffa, P., and Dominguez, R. (2002). Crystal structures of the vitamin D-binding protein and its complex with actin: structural basis of the actin-scavenger system. Proc. Natl. Acad. Sci. USA *99*, 8003–8008.

Pardee, J.D., and Spudich, J.A. (1982). Purification of muscle actin. Methods Cell Biol. *24*, 271–289.

Razzaq, A., Schmitz, S., Veigel, C., Molloy, J.E., Geeves, M.A., and Sparrow, J.C. (1999). Actin residue glu(93) is identified as an amino acid affecting myosin binding. J. Biol. Chem. *274*, 28321–28328.

Reichert, A., Heintz, D., Echner, H., Voelter, W., and Faulstich, H. (1996). Identification of contact sites in the actin-thymosin beta 4 complex by distance-dependent thiol cross-linking. J. Biol. Chem. *271*, 1301–1308.

Robbens, J., Louahed, J., De Pestel, K., Van Colen, I., Ampe, C., Vandekerckhove, J., and Renauld, J.C. (1998). Murine adseverin (D5), a novel member of the gelsolin family, and murine adseverin are induced by interleukin-9 in T-helper lymphocytes. Mol. Cell Biol. *18*, 4589–4596.

Robinson, R.C., Mejillano, M., Le, V.P., Burtnick, L.D., Yin, H.L., and Choe, S. (1999). Domain movement in gelsolin: a calcium-activated switch. Science *286*, 1939–1942.

Rommelaere, H., Van Troys, M., Gao, Y., Melki, R., Cowan, N.J., Vandekerckhove, J., and Ampe, C. (1993). Eukaryotic cytosolic chaperonin contains t-complex polypeptide 1 and seven related subunits. Proc. Natl. Acad. Sci. USA *90*, 11975–11979.

Rommelaere, H., De Neve, M., Melki, R., Vandekerckhove, J., and Ampe, C. (1999). The cytosolic class II chaperonin CCT recognizes delineated hydrophobic sequences in its target proteins. Biochemistry *38*, 3246–3257.

Safer, D. (1989). An electrophoretic procedure for detecting proteins that bind actin monomers. Anal. Biochem. *178*, 32–37.

Safer, D., Sosnick, T.R., and Elzinga, M. (1997). Thymosin beta 4 binds actin in an extended conformation and contacts both the barbed and pointed ends. Biochemistry *36*, 5806–5816.

Schagger, H., and von Jagow, G. (1987). Tricine-sodium dodecyl sulfate-polyacrylamide gel electrophoresis for the separation of proteins in the range from 1 to 100 kDa. Anal. Biochem. *166*, 368–379.

Schutt, C.E., Myslik, J.C., Rozycki, M.D., Goonesekere, N.C., and Lindberg, U. (1993). The structure of crystalline profilin-beta-actin. Nature *365*, 810–816.

Steinmetz, M.O., Stoffler, D., Muller, S.A., Jahn, W., Wolpensinger, B., Goldie, K.N., Engel, A., Faulstich, H., and Aebi, U. (1998). Evaluating atomic models of F-actin with an undecagold-tagged phalloidin derivative. J. Mol. Biol. *276*, 1–6.

Vainberg, I.E., Lewis, S.A., Rommelaere, H., Ampe, C., Vandekerckhove, J., Klein, H.L., and Cowan, N.J. (1998). Prefoldin, a chaperone that delivers unfolded proteins to cytosolic chaperonin. Cell *93*, 863–873.

Wertman, K.F., Drubin, D.G., and Botstein, D. (1992). Systematic mutational analysis of the yeast ACT1 gene. Genetics *132*, 337–350.